nature photonics

ARTICLES

https://doi.org/10.1038/s41566-021-00831-w

Optically synchronized fibre links using spectrally pure chip-scale lasers

Grant M. Brodnik[1], Mark W. Harrington[1], John H. Dallyn[2], Debapam Bose[1], Wei Zhang[3,7], Liron Stern[3,8], Paul A. Morton[4], Ryan O. Behunin[2,5], Scott B. Papp[3,6] and Daniel J. Blumenthal[1]✉

Precision optical-frequency and phase synchronization over fibre is critical for a variety of applications, from timekeeping to quantum optics. Such applications utilize ultra-coherent sources based on stabilized table-top laser systems. Chip-scale versions of these systems may dramatically broaden the application landscape by reducing the cost, size and power of such exquisite sources. Links based on the required narrow-linewidth integrated lasers, compact reference cavities and control methodologies have not yet been presented. Here, we demonstrate an optically synchronized link that achieves an ultralow residual phase error variance of 3×10^{-4} rad^2 at the receiver, using chip-scale stabilized lasers with laser linewidth of ~30 Hz and instability below 2×10^{-13} at 50 ms. This performance is made possible with integrated Brillouin lasers, compact reference cavities and a novel low-bandwidth optical-frequency-stabilized phase-locked loop. These results demonstrate a path towards low-power, precision applications including distributed atomic clocks, quantum links, database synchronization and digital-signal-processor-free coherent fibre interconnects.

The distribution of precision optical frequency and phase references over fibre-optic links[1–4] enables applications such as high-precision metrology, investigation of variations in fundamental physical constants[5], interferometry for radio astronomy[6], optical clock comparison[7–10] and high-capacity coherent communications[11]. To achieve high precision, scientific applications employ ultralow-linewidth, frequency-stabilized lasers[12,13], requiring sophisticated laser systems at the table-top scale. At the same time, applications like coherent fibre communications use power-intensive digital signal processors (DSPs)[14–16] to achieve phase synchronization with lower-cost and less stable lasers. Miniaturization of stable laser technologies would broaden the use of optically synchronized fibre links to a wider range of applications, including distributed network synchronization[17], precision time protocols[18,19] and deployable optical clock networks[10], as well as enabling new approaches to realizing energy-efficient, DSP-free, high-capacity coherent fibre-optic interconnects[20,21].

Optical frequency and phase synchronization can be accomplished using electronic phase-locked loops (EPLLs)[22,23], optical phase-locked loops (OPLLs)[24–28] and DSPs[14–16]. Several factors drive how well these techniques scale in terms of performance, complexity and power consumption at optical carrier frequencies, including laser and fibre phase noise and stability, modulation bandwidth, feedback loop noise, bandwidth requirements and high-frequency analogue and digital electronics. Compact, ultralow-linewidth, stabilized lasers with ultralow phase noise can enable circuitry normally associated with coherent radiofrequency (RF) and wireless communications to support links at optical frequencies. Examples of low-bandwidth feedback techniques used in precision scientific experiments include the Pound–Drever–Hall (PDH)[29] method coupled with thermally engineered glass or single-crystal high-Q optical reference cavities[12,13] housed in sophisticated environmental isolation systems. These state-of-the-art, laboratory-scale lasers are capable of linewidths below 10 mHz with a carrier instability of 4×10^{-17} at timescales between one and a few tens of seconds[13]. Chip-scale stabilized lasers with exceptional phase noise and frequency stability have been realized by locking semiconductor or stimulated Brillouin scattering (SBS) lasers to whispering-gallery-mode resonators[30,31], photonic integrated spiral waveguides[32] and compact Fabry–Pérot resonators[33]. However, so far, the use of independent, ultralow-linewidth, stable sources in a precision fibre frequency link and the demonstration of ultralow residual phase error using low-bandwidth synchronization methods have not been reported.

In this Article, we demonstrate precision phase-locked optical sources over a fibre link using independent, mutually coherent lasers that are frequency-stabilized at the chip scale. The fibre-connected lasers are phase-synchronized with a low residual phase error variance[25] of 3×10^{-4} rad^2 for a homodyne lock, orders of magnitude lower than achieved with OPLLs employing large-linewidth integrated lasers[24–28]. This performance is achieved by consideration of frequency noise and drift contributions from the integrated lasers, a compact reference cavity and optical fibre, as well as feedback loop and lock dynamics. We combine these stabilized, spectrally pure, independent chip-scale lasers with an optical-frequency-stabilized phase-locked loop (OFS-PLL) to provide precise synchronization using only low-bandwidth feedback loops (<800 kHz), without the need for the high-bandwidth electronics of EPLL or OPLL circuits or power-intensive DSPs. The lasers have a cavity-stabilized SBS laser (CS-SBS) design, consisting of a photonic integrated silicon nitride (SiN) SBS laser[34] locked to a compact silica Fabry–Pérot optical reference cavity[33]. We measure the optical frequency noise (FN) of the transmit (Tx) and receive (Rx) lasers, as well as the heterodyne beat note spectrum between these lasers, resulting in an integral linewidth of ~30 Hz for each CS-SBS laser and a fractional

[1]Department of Electrical and Computer Engineering, University of California Santa Barbara, Santa Barbara, CA, USA. [2]Department of Applied Physics and Materials Science, Northern Arizona University, Flagstaff, AZ, USA. [3]Time and Frequency Division 688, National Institute of Standards and Technology, Boulder, CO, USA. [4]Morton Photonics, West Friendship, MD, USA. [5]Center for Materials Interfaces in Research and Applications (MIRA), Northern Arizona University, Flagstaff, AZ, USA. [6]Department of Physics, University of Colorado Boulder, Boulder, CO, USA. [7]Present address: Jet Propulsion Laboratory, Pasadena, CA, USA. [8]Present address: Department of Applied Physics, Hebrew University of Jerusalem, Jerusalem, Israel. ✉e-mail: danb@ucsb.edu

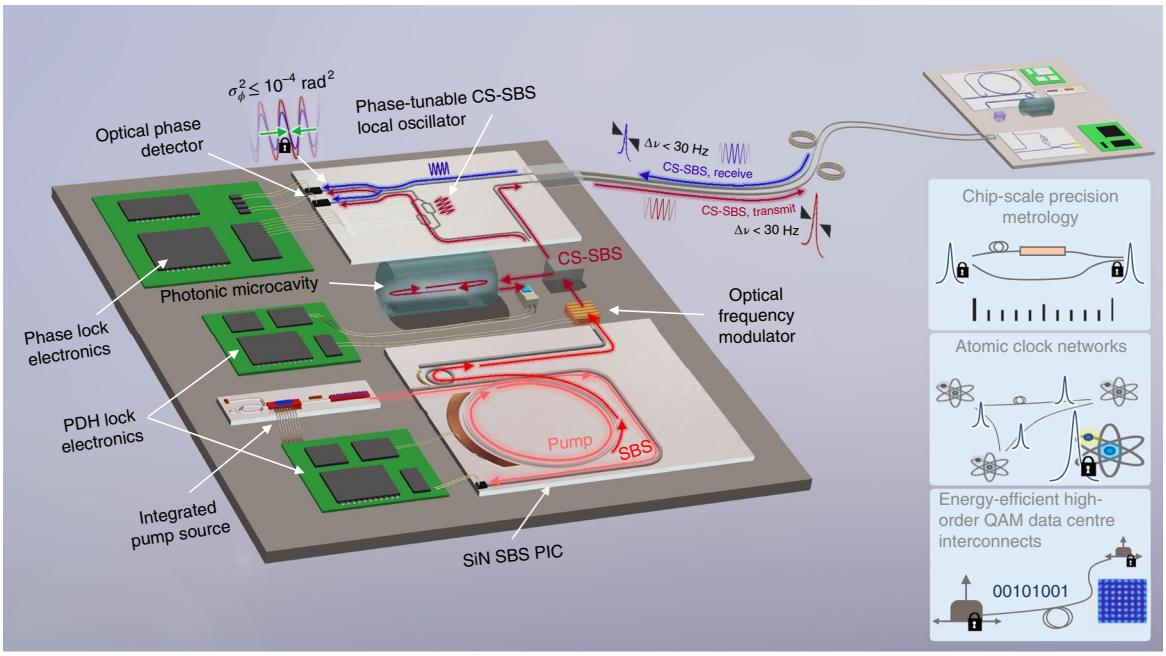

Fig. 1 | Optically synchronized precision fibre link. A precision optical-frequency synchronized fibre link can be realized with independent CS-SBS lasers. SBS lasing is performed using an ultralow-optical-loss SiN photonic integrated circuit (PIC)[34] for first-stage phase noise reduction of the fundamental linewidth to <1 Hz. Carrier stabilization is implemented with low-bandwidth sub-megahertz PDH feedback loops and locking to a compact reference cavity with quality factor (Q) of one billion. The CS-SBS laser sources provide stable carriers for a low-bandwidth OFS-PLL. This type of compact, carrier-stable link will enable applications in precision metrology, distributed atomic timekeeping and high-capacity coherent fibre-optic communications.

frequency instability (FFI) of 2×10^{-13} at 50 ms for the open-loop heterodyne beat note. For the homodyne phase lock, the low residual phase error is achieved with received optical powers as low as −34 dBm and is estimated to support coherent quadrature amplitude modulation (QAM) out to 256-QAM[11]. For future data-centre interconnects, these results show promise for efficient carrier phase recovery in QAM links, in contrast to DSP[14–16] approaches, which can consume an estimated several watts per several hundred gigabits per second[23], and offer better performance at lower loop bandwidths and power consumption than integrated OPLLs[24–28]. These results represent a major leap towards deploying chip-scale stabilized photonic integrated lasers for applications requiring precision carrier and phase recovery over fibre links without high-power, high-bandwidth analogue electronics or DSPs.

Results

Precision fibre link and node architecture. A chip-scale, optically synchronized link is shown in Fig. 1, which shows a CS-SBS source used for the Tx and Rx lasers at the fibre link end points. The CS-SBS design[34] comprises a tunable semiconductor pump laser[35] locked to a SiN-waveguide SBS laser using a low-bandwidth PDH[29] lock optoelectronic loop. The SBS laser output is modulated by an acousto-optic modulator (AOM) to generate the optical carrier to be stabilized. The AOM is driven by a voltage-controlled oscillator (VCO) that aligns and locks the optical carrier to a resonance of the compact silica reference cavity using a second low-bandwidth PDH lock circuit. This reference cavity lock stabilizes the SBS optical carrier and reduces the laser phase noise and integral linewidth within a loop bandwidth of several hundred kilohertz[33]. The stabilized CS-SBS emission is split to create a transmitted carrier and a receiver-side tunable optical local oscillator. The laser output is coupled to the fibre-optic link and transmitted to a receiving node with a second independent CS-SBS laser of the same design. The incoming signal is optically mixed with a single-sideband-modulated local oscillator CS-SBS laser. This photomixed signal serves as the error signal for a homodyne optical phase lock[24]. The error signal is filtered by a proportional-integral^2-derivative (PI^{2}D) loop filter with integral poles at 50 kHz and 100 kHz, and fed back to the local oscillator tuning control to close the phase lock, completing the OFS-PLL. The high mutual coherence between Tx and Rx lasers results in ultralow residual phase error and improved phase lock capture- and hold-in range over a non-stabilized link. The linewidth reduction properties of the SBS laser reduce the mutual phase noise at frequency offsets outside the bandwidth of the final optical phase lock.

Linewidth-narrowed, cavity-stabilized optical carriers. The CS-SBS laser is shown in detail in Fig. 2. Linewidth narrowing occurs in two stages, with the second stage also performing carrier stabilization. In the first stage, the SBS laser reduces the semiconductor pump laser fundamental linewidth from ~60 Hz to just over 1 Hz (refs. [34,36]). The pump laser is locked to an SBS cavity resonance using a sub-megahertz-bandwidth PDH loop. The first-order Stokes SBS emission has frequency noise of 10 Hz^2 Hz^{-1} at offsets near 100 kHz, dropping to ~1 Hz^2 Hz^{-1} at offsets greater than 1 MHz from the carrier.

For the second stage of linewidth reduction and carrier stabilization, we utilized a compact, 25.4-mm Fabry–Pérot cavity with Q greater than one billion, housed in a vibration- and temperature-isolation enclosure[33]. Stabilization to this cavity reduces SBS frequency noise within the bandwidth of the PDH lock, where environmental and technical sources, as well as the conversion of erbium-doped fibre-amplifier-induced pump relative intensity noise to photothermal noise[32,37,38] inside the SBS cavity, dominate. The thermal mass of the cavity is sufficiently large to yield a time constant for thermal conduction to the environment on the order of 5 min, and therefore it does not respond directly to external macroscopic control on the timescale of these frequency noise sources (for example, changing the temperature of the reference cavity). The control loop must actively tune the optical frequency in the

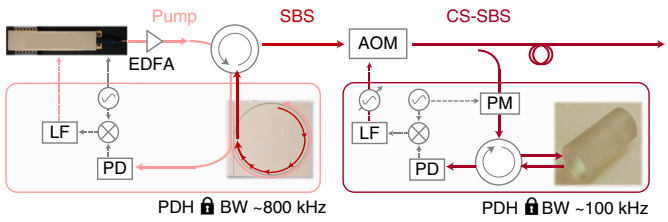

Fig. 2 | The CS-SBS laser. An external fibre cavity diode laser (ECDL)[35] is optically amplified using an erbium-doped fibre amplifier (EDFA) to serve as the pump for an integrated SBS laser. The SBS laser[34] is stabilized to the compact reference cavity[33] using an AOM optical frequency shifter and a variable-frequency VCO. PDH loops incorporate phase modulators (PMs), VCOs, photodiodes (PDs), electronic mixers and low-bandwidth (BW) loop filters (LFs).

low- to mid-frequency range of several hundred kilohertz. The PDH error signal is processed by a PI²D loop filter and controls the frequency of the VCO that drives the AOM. When the optical frequency shift necessary to lock to the reference cavity approaches the maximum AOM tuning range, the temperature of the SiN SBS laser is adjusted to coarsely re-centre the optical carrier. The result is a low-bandwidth PDH loop that reduces SBS laser frequency noise within the loop bandwidth by more than three orders of magnitude, from ~10^4 to ~10^1 $Hz^2\,Hz^{-1}$.

Frequency noise, linewidth and stability. Independent CS-SBS lasers were connected over 200 m of fibre (Fig. 3a). We characterized the laser frequency noise at each node and the open-loop heterodyne beat note at the Rx (Fig. 3b–d). The following parameters were extracted (these are described further in the Methods): fundamental linewidth (FLW), integral linewidth (ILW) and Allan deviation (ADEV) of the FFI. Optical frequency noise was measured using a RF-calibrated fibre-based asymmetric Mach–Zehnder interferometer (aMZI) as an optical frequency discriminator (OFD). The OFD measurements are valid down to offsets of 10 kHz, at which fibre noise in the aMZI dominates. Below the 10 kHz offset, we used an electrical frequency discriminator[39] (EFD) to measure the frequency noise of the heterodyne beat note between the Tx and Rx pump, SBS and CS-SBS lasers, capturing the combined noise dynamics of each independent optical source. The heterodyne beat note noise trace over the 1 Hz to 10 MHz range was obtained by stitching the frequency noise of the Tx and Rx OFD traces (Fig. 3b,c) with their respective EFD measurements, as shown in Fig. 3d. Further details of the OFD and EFD measurements are provided in the Methods and in Supplementary Section II.

The FLWs of the Rx and Tx pump lasers (light blue and light red, respectively, in Fig. 3b,c) were measured at ~60 Hz. After the SBS lasing stage, the Rx and Tx SBS laser (medium blue and medium red, respectively, in Fig. 3b,c) FLWs were reduced to 1.0 Hz and 2.4 Hz, respectively. After laser stabilization, the measured FLWs of the Rx and Tx CS-SBS (dark blue and dark red, respectively, in Fig. 3b,c) lasers increased to 3.4 Hz and 3.9 Hz, respectively. Servo bumps as the phase approached 180° and positive feedback near the loop bandwidths in the cavity lock loops at ~50 kHz and ~100 kHz, due to the different AOMs and electronics with different control bandwidths used in the experiments, were observed for the Tx and Rx CS-SBS lasers, respectively.

To understand the fundamental limits of cavity stabilization on CS-SBS frequency noise, we simulated the SBS stabilization stage using an ideal PDH lock by mapping experimental SBS frequency noise through a PI²D feedback loop with poles matched to those used in the experiment. The laser noise closely tracked the cavity frequency reference and the simulated CS-SBS (green curve in Fig. 3d) in-loop frequency noise was limited only by the cavity fundamental thermal noise. This simulation is presented in more detail in Supplementary Section I. We calculated the ILW of the heterodyne beat note signals using the β-separation method[40] and by integrating phase noise from high offset frequencies down to the frequency offset at which the integrated phase noise equalled $1/\pi$ rad^2 (refs. [22,30]). The calculated ILW of the beat note between Tx and Rx pump lasers was reduced from 133 kHz (β-separation) and 2.97 kHz ($1/\pi$) to 104 Hz (β-separation) and 43 Hz ($1/\pi$) for the CS-SBS laser beat note. Assuming Gaussian lineshapes and an equal contribution by each CS-SBS laser to the heterodyne 43-Hz ($1/\pi$) ILW[41], each independent optical ILW was estimated to be ~30 Hz. The pump, SBS and CS-SBS linewidths are summarized in Supplementary Table 1. The beat note ADEV is shown in Fig. 3e, reaching a minimum of 2×10^{-13} at 50 ms with a linear drift of 803 $Hz\,s^{-1}$ starting to appear at ~50 ms (thermorefractive drift between cavities due to temperature changes in the laboratory). Additional ADEV details are provided in Supplementary Section III.

Precision, optically synchronized fibre link. The OFS-PLL (Fig. 4a) synchronizes the optical phase between two independent CS-SBS lasers connected by 200 m of optical fibre. The Tx and Rx signals were photomixed on a balanced photodetector (BPD) with bandwidth of 45 MHz to generate a homodyne phase error signal[24]. The tunable local oscillator (LO) for homodyne phase locking was generated using a PI²D filtered phase error signal to control a 6-GHz VCO-driven optical phase modulator and an optical filter to select the upper sideband.

In open-loop operation, the phase error signal is the heterodyne beat note of the two CS-SBS lasers with the measured frequency noise characteristics shown previously in Fig. 3d, oscillating at the difference frequency of the Tx and Rx optical carriers. After engaging the phase lock, a digital oscilloscope is used to verify a zero-fringe-slip transition to closed-loop operation[42] (Fig. 4b). We estimate a phase lock acquisition range of 700 kHz, which can be increased in future designs with a frequency pull-in loop. The phase noise power spectral density (PSD), $S_\phi(f)$, of the in-loop phase error signal (received optical power of −14 dBm) is shown in Fig. 4c. The servo bumps from the CS-SBS cavity lock stages near ~40 kHz, and at ~1 MHz near the OFS-PLL bandwidth, are evident. Line noise from electronics and power supplies is seen at multiples of 60 Hz. We plot three curves (purple) representing summed, uncorrelated phase noise of two lasers having FLWs of 1, 10 and 100 Hz (frequency noise described by white noise only) to show the benefit of SBS lasing to reduce the laser FLW for low phase noise at high-frequency offsets. Residual phase error variances, σ_ϕ^2, calculated by integrating the $S_\phi(f)$ curve of Fig. 4c over several frequency sub-spans from an offset of 1 Hz up to the photodiode bandwidth of 45 MHz, are summarized in Fig. 4d. The residual phase error variances are plotted over a span of 20 min for multiple received optical powers between −14 dBm and −44 dBm in Fig. 4e. At a low received signal optical power of −44 dBm, the residual phase error increased to ~8×10^{-4} rad^2.

We estimated the performance of the OFS-PLL in a coherent link by relating the measured residual phase error to phase errors that can be tolerated for forward error correction (FEC)[43] thresholds for high-order QAM, as shown in Fig. 4e. We calculated the minimum phase angle separation for nearest-neighbour QAM symbols[11] and the resulting phase error thresholds for various modulation orders (M) and extended this result to a symbol error rate, assuming high optical signal-to-noise ratio (OSNR) and Gaussian-distributed phase noise. The measured OFS-PLL residual phase error variance of 3×10^{-4} rad^2 is sufficient for at least 256-QAM transmission, for example, below the 400ZR C-FEC[43] bit error rate of 1.25×10^{-2} in a phase-noise-limited link using this estimation. In a low OSNR regime, phase noise is not the only consideration for link

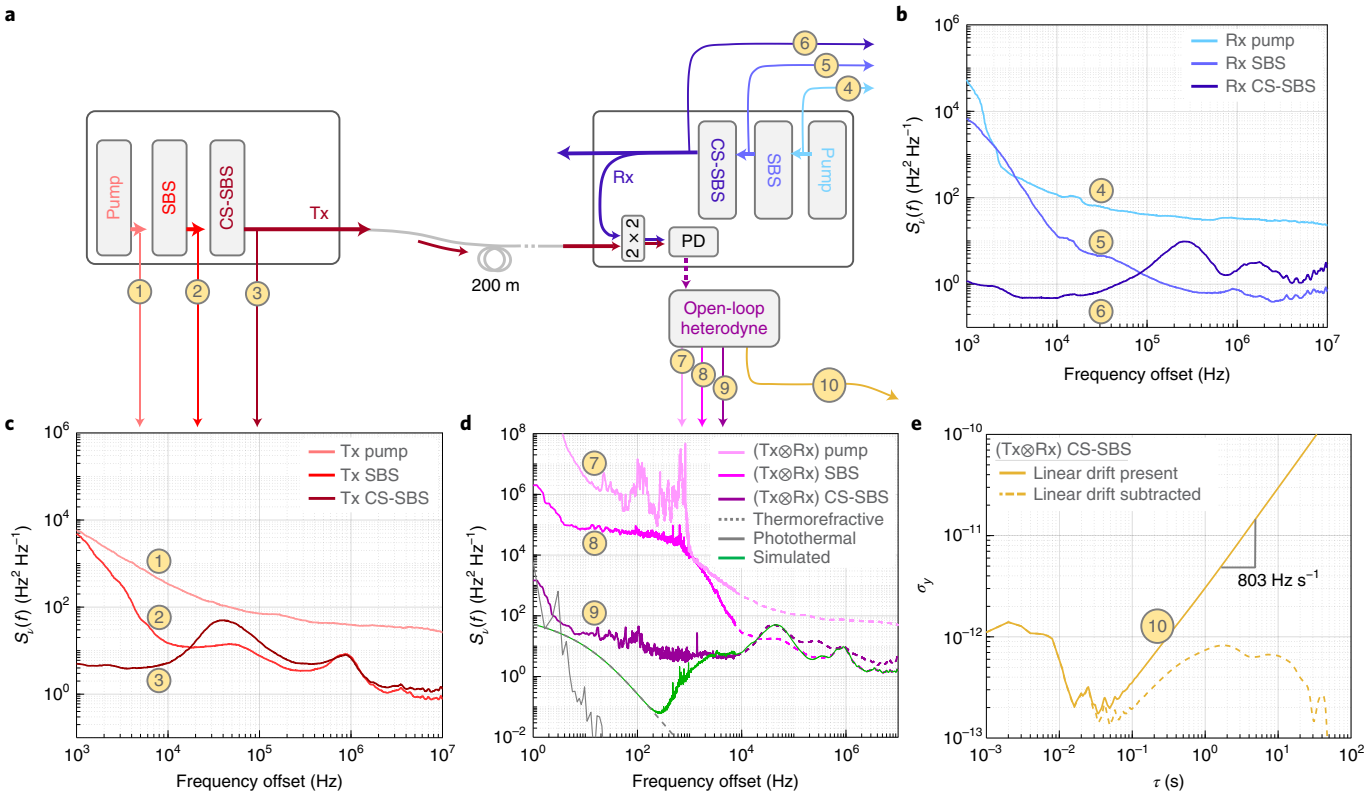

Fig. 3 | Laser carrier and heterodyne beat note linewidth and stability measurements. a, Two independent CS-SBS lasers (transmit, Tx; receive, Rx) are connected by optical fibre and photomixed at the receiver PD, yielding a heterodyne beat note signal. The measurement locations of the FN ($S_\nu(f)$) of the transmitted and received pump, SBS and CS-SBS optical carriers and receiver-side heterodyne beat notes of pump, SBS and CS-SBS are labelled 1 to 10 and are identified in the plots in **b**–**e**. **b**, The FN of the independent Rx optical carriers as measured with an OFD. **c**, The Tx FN measured with OFD. **d**, Tx–Rx open-loop heterodyne beat notes measured with an EFD. Dashed lines are the sum of the FN of the independent optical carriers from **b** and **c** for each configuration. The cavity thermal noise limit (grey dashed line) and photothermal noise (grey solid line) are also shown. The simulated FN of a CS-SBS laser limited by cavity thermal noise is shown in green. **e**, Overlapping ADEV of the FFI of the CS-SBS heterodyne beat note referenced to a carrier frequency of 193 THz, with a relative linear drift of 803 Hz s^{-1} between reference cavities present (solid line) and with the drift subtracted (dashed line).

performance, and requirements for residual phase error variance are more stringent[44]. Further details of this approximation are provided in Supplementary Section V.

Discussion

We have demonstrated a high-precision optical carrier synchronized fibre link with low residual phase error variance based on independent chip-scale mutually coherent stabilized lasers. The ability to provide this degree of phase synchronization on a 193-THz optical carrier using low-bandwidth electronics typical of RF links opens the door to new applications for precision optical-frequency-synchronized fibre links. By combining the phase noise reduction dynamics of SBS with the inherent stability of a compact one-billion-Q reference cavity, we achieve a 43-Hz heterodyne beat note ILW and FFI better than 2×10^{-13} at 50 ms with independent optical sources, over a 200-m fibre-optic link. We have used a novel OFS-PLL that delivers a residual phase error variance of 3×10^{-4} rad^2 with a loop bandwidth ~800 kHz and received optical power of −34 dBm. This performance is achievable for fibre lengths up to ~150 km, at which point contributions from low-frequency fibre phase noise, primarily driven by environmental sources[4], surpass the cavity stabilization noise and impact the phase lock performance. At high frequencies offset from the carrier, fundamental noise from thermomechanical and thermoconductive sources[45] will surpass that of the CS-SBS laser and dominate the SBS laser high-frequency noise. At these high-frequency offsets, performance will be dominated by fibre noise at lengths beyond ~300 km (further details are provided in Supplementary Section VI).

In the future, individual OFS-PLL components could be readily integrated into SiN and heterogeneous silicon photonic platforms[46–48] with milliwatt-tier bipolar CMOS electrical circuits. We estimate this will require several hundred milliwatts for silicon-photonic optical-frequency tuning[46]. The current demonstration employs bulk thermoelectric coolers for thermal control (consuming 148 mW) and discrete components for optical-frequency tuning and amplification. Integration can mitigate this power consumption by heterogeneously integrating the SBS pump source[49,50], reference cavities[51,52], semiconductor optical amplifiers, waveguide heaters and co-located control electronics[46]. Other future directions can include adding a frequency pull-in stage to extend the capture range of the optical phase lock and operating with both polarizations to enable polarization-diverse sensing and optical communications. Additionally, the OFS-PLL will have advantages in high-order coherent optical communications with favourable power scaling and loop electronics that do not depend on symbol rate, in contrast to conventional DSPs. The photonic integrated CS-SBS laser source can serve as a single low-noise pump for integrated optical nonlinear microresonators to realize high-spectral-purity optical-frequency combs at the chip scale[53]. Such techniques will enable amortization of complexity, cost and power consumption across many wavelengths. These results show promise for new applications that require ultrahigh-spectral-purity laser sources and precision optical

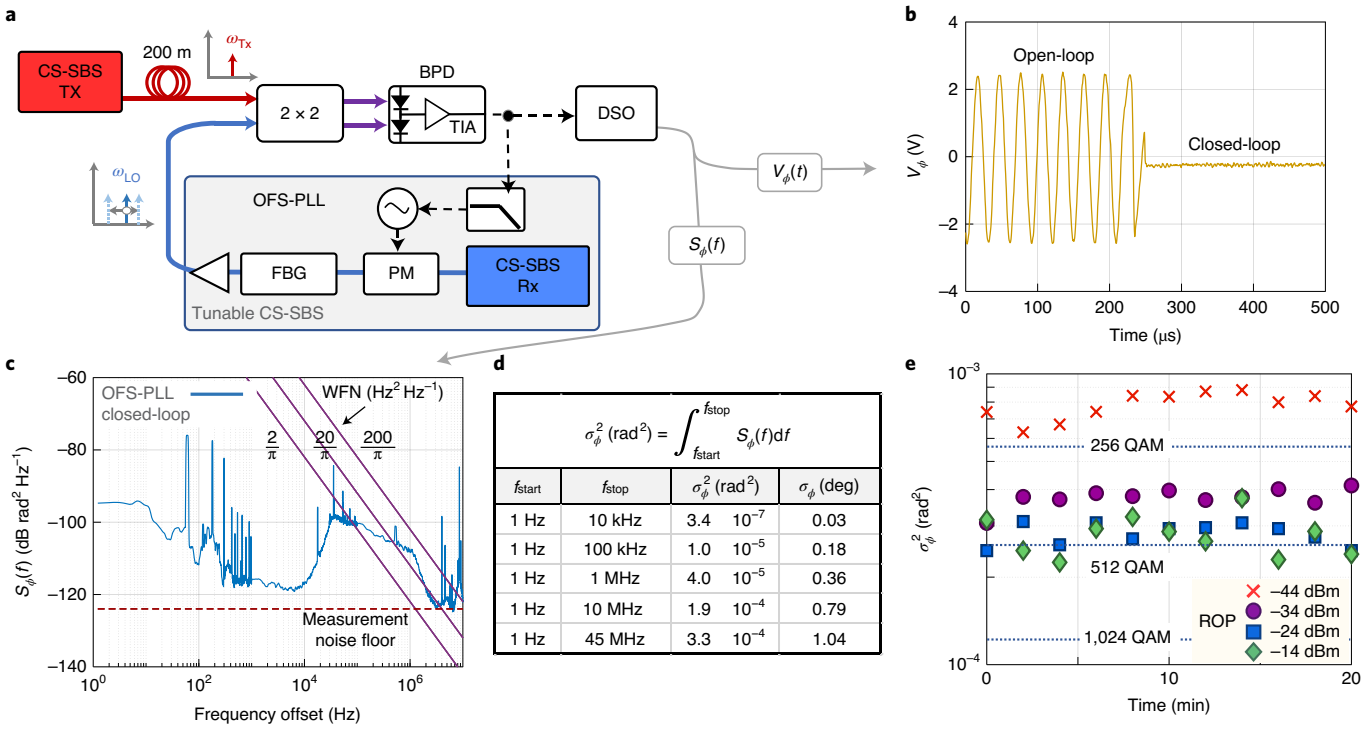

f_{start}	f_{stop}	σ_ϕ^2 (rad²)	σ_ϕ (deg)
1 Hz	10 kHz	3.4×10^{-7}	0.03
1 Hz	100 kHz	1.0×10^{-5}	0.18
1 Hz	1 MHz	4.0×10^{-5}	0.36
1 Hz	10 MHz	1.9×10^{-4}	0.79
1 Hz	45 MHz	3.3×10^{-4}	1.04

Fig. 4 | Precision link operation and performance. a, A CS-SBS laser transmits (Tx) a linewidth-narrowed, stable optical carrier over fibre. A receiver (Rx) CS-SBS laser is made tunable by optically filtering (via a fibre Bragg grating, FBG) a PM sideband driven by a VCO with a control signal derived from a BPD (bandwidth, 45 MHz) with built-in transimpedance amplifier (TIA) as an optical phase detector[24]. **b**, A digital oscilloscope (DSO) time trace of the OFS-PLL phase error signal, demonstrating open- and closed-loop homodyne phase lock operation. **c**, OFS-PLL phase noise PSD measured at the phase detector. Reference lines corresponding to the summed uncorrelated noise of two lasers with FLWs (only white frequency noise, WFN) of 1 Hz, 10 Hz and 100 Hz are shown in purple. **d**, The residual phase error variance, σ_ϕ^2, found by integrating $S_\phi(f)$ over various frequency spans. **e**, σ_ϕ^2 over multiple 20-min timescales for varied CS-SBS received optical power (ROP) at the phase detector. Approximated high-order QAM thresholds for the required phase error variance in a high-OSNR phase-noise-limited link are shown as dotted lines.

phase in compact, low-power implementations, such as distributed atomic clocks for timing and metrology and energy-efficient DSP-free terabits per second (Tbps) coherent optical links in data-centre interconnects.

Online content

Any methods, additional references, Nature Research reporting summaries, source data, extended data, supplementary information, acknowledgements, peer review information; details of author contributions and competing interests; and statements of data and code availability are available at https://doi.org/10.1038/s41566-021-00831-w.

Received: 24 December 2020; Accepted: 17 May 2021;
Published online: 21 June 2021

References

1. Ma, L.-S., Jungner, P., Ye, J. & Hall, J. L. Delivering the same optical frequency at two places: accurate cancellation of phase noise introduced by an optical fiber or other time-varying path. *Opt. Lett.* **19**, 1777–1779 (1994).
2. Hall, J. L. & Zhu, M. in *International School of Physics Enrico Fermi Course CXVII, Laser Manipulation of Atoms and Ions* (eds Arimondo, E. et al.) 671–702 (North Holland, 1993).
3. Foreman, S. M. et al. Coherent optical phase transfer over a 32-km fiber with 1-s instability at 10^{-17}. *Phys. Rev. Lett.* **99**, 153601 (2007).
4. Calonico, D. et al. High-accuracy coherent optical frequency transfer over a doubled 642-km fiber link. *Appl. Phys. B* **117**, 979–986 (2014).
5. Roberts, B. M. et al. Search for transient variations of the fine structure constant and dark matter using fiber-linked optical atomic clocks. *New J. Phys.* **22**, 093010 (2020).
6. Clivati, C. et al. A coherent fiber link for very long baseline interferometry. *IEEE Trans. Ultrason. Ferroelectr. Freq. Control* **62**, 1907–1912 (2015).
7. Grotti, J. et al. Geodesy and metrology with a transportable optical clock. *Nat. Phys.* **14**, 437–441 (2018).
8. Lisdat, C. et al. A clock network for geodesy and fundamental science. *Nat. Commun.* **7**, 12443 (2016).
9. Fujieda, M. et al. All-optical link for direct comparison of distant optical clocks. *Opt. Express* **19**, 16498–16507 (2011).
10. Riehle, F. Optical clock networks. *Nat. Photon.* **11**, 25–31 (2017).
11. Nakazawa, M., Hirooka, T., Yoshida, M. & Kasai, K. in *Optical Fiber Telecommunications* 6th edn (eds Kaminow, I. P. et al.) 297–336 (Academic Press, 2013).
12. Kessler, T. et al. A sub-40-mHz-linewidth laser based on a silicon single-crystal optical cavity. *Nat. Photon.* **6**, 687–692 (2012).
13. Matei, D. G. et al. 1.5-μm lasers with sub-10-mHz linewidth. *Phys. Rev. Lett.* **118**, 263202 (2017).
14. Pillai, B. S. G. et al. End-to-end energy modeling and analysis of long-haul coherent transmission systems. *J. Lightw. Technol.* **32**, 3093–3111 (2014).
15. Crivelli, D. E. et al. Architecture of a single-chip 50-Gb/s DP-QPSK/BPSK transceiver with electronic dispersion compensation for coherent optical channels. *IEEE Trans. Circuits Syst. Regul. Pap.* **61**, 1012–1025 (2014).
16. Laperle, C. & O'Sullivan, M. Advances in high-speed DACs, ADCs and DSP for optical coherent transceivers. *J. Lightw. Technol.* **32**, 629–643 (2014).
17. Corbett, J. C. et al. Spanner: Google's globally-distributed database. In *OSDI (2012)* 251–264 (USENIX Association, 2012).
18. Dierikx, E. F. et al. White rabbit precision time protocol on long-distance fiber links. *IEEE Trans. Ultrason. Ferroelectr. Freq. Control* **63**, 945–952 (2016).
19. Schediwy, S. W., Gozzard, D. R., Stobie, S., Malan, J. A. & Grainge, K. Stabilized microwave-frequency transfer using optical phase sensing and actuation. *Opt. Lett.* **42**, 1648–1651 (2017).
20. Brodnik, G. M. et al. Chip-scale, optical-frequency-stabilized PLL for DSP-free, low-power coherent QAM in the DCI. In *Optical Fiber Communication Conference (OFC) 2020* M3A.6 (OSA, 2020).

21. Blumenthal, D. J. et al. Frequency-stabilized links for coherent WDM fiber interconnects in the datacenter. *J. Lightw. Technol.* **38**, 3376–3386 (2020).
22. Kikuchi, K. Fundamentals of coherent optical fiber communications. *J. Lightw. Technol.* **34**, 157–179 (2016).
23. Perin, J. K., Shastri, A. & Kahn, J. M. Design of low-power DSP-free coherent receivers for data center links. *J. Lightw. Technol.* **35**, 4650–4662 (2017).
24. Kazovsky, L. G. Balanced phase-locked loops for optical homodyne receivers: performance analysis, design considerations and laser linewidth requirements. *J. Lightw. Technol.* **4**, 182–195 (1986).
25. Satyan, N. Phase noise reduction of a semiconductor laser in a composite optical phase-locked loop. *Opt. Eng.* **49**, 124301 (2010).
26. Balakier, K., Ponnampalam, L., Fice, M. J., Renaud, C. C. & Seeds, A. J. Integrated semiconductor laser optical phase lock loops. *IEEE J. Sel. Top. Quantum Electron.* **24**, 1–12 (2018).
27. Simsek, A. et al. Evolution of chip-scale heterodyne optical phase-locked loops toward Watt level power consumption. *J. Lightw. Technol.* **36**, 258–264 (2018).
28. Park, H. et al. 40-Gbit/s coherent optical receiver using a Costas loop. *Opt. Express* **20**, 9736–9741 (2012).
29. Drever, R. W. P. et al. Laser phase and frequency stabilization using an optical resonator. *Appl. Phys. B Photophys. Laser Chem.* **31**, 97–105 (1983).
30. Liang, W. et al. Ultralow noise miniature external cavity semiconductor laser. *Nat. Commun.* **6**, 7371 (2015).
31. Loh, W. et al. Dual-microcavity narrow-linewidth Brillouin laser. *Optica* **2**, 225–232 (2015).
32. Lee, H. et al. Spiral resonators for on-chip laser frequency stabilization. *Nat. Commun.* **4**, 2468 (2013).
33. Zhang, W. et al. Ultranarrow linewidth photonic-atomic laser. *Laser Photon. Rev.* **14**, 1900293 (2020).
34. Gundavarapu, S. et al. Sub-hertz fundamental linewidth photonic integrated Brillouin laser. *Nat. Photon.* **13**, 60–67 (2019).
35. Morton, P. A. & Morton, M. J. High-power, ultra-low noise hybrid lasers for microwave photonics and optical sensing. *J. Lightw. Technol.* **36**, 5048–5057 (2018).
36. Debut, A., Randoux, S. & Zemmouri, J. Linewidth narrowing in Brillouin lasers: theoretical analysis. *Phys. Rev. A* **62**, 023803 (2000).
37. Loh, W. et al. A microrod-resonator Brillouin laser with 240-Hz absolute linewidth. *New J. Phys.* **18**, 045001 (2016).
38. Matsko, A. B., Savchenkov, A. A., Yu, N. & Maleki, L. Whispering-gallery-mode resonators as frequency references. I. Fundamental limitations. *J. Opt. Soc. Am. B* **24**, 1324–1335 (2007).
39. Schilt, S. et al. Frequency discriminators for the characterization of narrow-spectrum heterodyne beat signals: application to the measurement of a sub-hertz carrier-envelope-offset beat in an optical frequency comb. *Rev. Sci. Instrum.* **82**, 123116 (2011).
40. Di Domenico, G., Schilt, S. & Thomann, P. Simple approach to the relation between laser frequency noise and laser line shape. *Appl. Opt.* **49**, 4801–4807 (2010).
41. Nazarathy, M., Sorin, W. V., Baney, D. M. & Newton, S. A. Spectral analysis of optical mixing measurements. *J. Lightw. Technol.* **7**, 1083–1096 (1989).
42. Kazovsky, L. G. & Atlas, D. A. A 1,320-nm experimental optical phase-locked loop: performance investigation and PSK homodyne experiments at 140 Mb/s and 2 Gb/s. *J. Lightw. Technol.* **8**, 1414–1425 (1990).
43. Sluyski, M. A., Gass, K. & Stauffer, D. R. *Implementation Agreement 400ZR OI-400ZR-01.0* (Optical Internetworking Forum, 2020).
44. Ip, E., Lau, A. P. T., Barros, D. J. F. & Kahn, J. M. Coherent detection in optical fiber systems. *Opt. Express* **16**, 753–791 (2008).
45. Duan, L. General treatment of the thermal noises in optical fibers. *Phys. Rev. A* **86**, 023817 (2012).
46. Idjadi, M. H. & Aflatouni, F. Nanophotonic phase noise filter in silicon. *Nat. Photon.* **14**, 234–239 (2020).
47. Blumenthal, D. J., Heideman, R., Geuzebroek, D., Leinse, A. & Roeloffzen, C. Silicon nitride in silicon photonics. *Proc. IEEE* **106**, 2209–2231 (2018).
48. Komljenovic, T. et al. Photonic integrated circuits using heterogeneous integration on silicon. *Proc. IEEE* **106**, 2246–2257 (2018).
49. Brodnik, G. M. et al. Ultra-narrow linewidth chip-scale heterogeneously integrated silicon/III–V tunable laser pumped Si/Si_3N_4 SBS laser. In *Conference on Lasers and Electro-Optics*, *OSA Technical Digest* STu3M.5 (Optical Society of America, 2020).
50. Huang, D. et al. High-power sub-kHz linewidth lasers fully integrated on silicon. *Optica* **6**, 745–752 (2019).
51. Zhao, Q. et al. Low-loss low thermo-optic coefficient Ta_2O_5 on crystal quartz planar optical waveguides. *APL Photonics* **5**, 116103 (2020).
52. Puckett, M. W. et al. 422 million intrinsic quality factor planar integrated all-waveguide resonator with sub-MHz linewidth. *Nat. Commun.* **12**, 934 (2021).
53. Harrington, M. W. et al. Kerr soliton microcomb pumped by an integrated SBS laser for ultra-low linewidth WDM sources. In *Optical Fiber Communication Conference* (*OFC*) *2020* T4G.6 (OSA, 2020); https://doi.org/10.1364/OFC.2020.T4G.6

Methods

Frequency noise of optical carriers. We directly measured the PSD of frequency fluctuations (frequency noise), $S_\nu(f)$, of independent optical sources using a calibrated, optical-fibre-based aMZI optical-frequency discriminator. Optical frequency fluctuations of the laser under test were converted into analogue voltage fluctuations, which were sampled by an analogue-to-digital converter (ADC) and processed offline for spectral characterization. The fibre-based aMZI consisted of a 200-m fibre delay in the asymmetric path and had a corresponding measured free spectral range of 1.026 MHz. The ADC sampling was performed using a real-time scope, triggered when the optical source was at the quadrature region of the aMZI transfer function. With known peak-to-peak voltage fluctuations, V_{pp}, and aMZI optical time delay, τ_D, the voltage PSD, $S_V(f)$ (in $V^2\,Hz^{-1}$), was converted to FN ($S_\nu(f)$, in $Hz^2\,Hz^{-1}$), as a function of carrier offset frequency f, by

$$S_\nu(f) = S_V(f)\left[\frac{f}{\sin(\pi f \tau_D)\,V_{pp}}\right]^2 \quad (1)$$

This aMZI transfer function conversion between PSDs results in artificial spurs at integer multiples of the aMZI free spectral range due to the sin(·) term in the denominator, which are removed with a median filter in the data-processing step. Additional details of the OFD measurements are provided in Supplementary Section II and schematically in Supplementary Fig. 1.

Frequency noise of the optical heterodyne beat note. The optical-frequency discriminator FN measurements are dominated by fibre and vibration noise in the optical delay path at carrier offset frequencies below ~10 kHz, requiring an additional method to accurately report $S_\nu(f)$ at low frequencies. We did this by optically mixing two lasers and measuring the frequency noise of the intermediate frequency (IF) signal with a MITEQ model FMDM EFD[39]. The voltage output scaled by the discriminator constant is the frequency error of the IF signal. The output was filtered with a fifth-order π-filter with bandwidth of 200 kHz to prevent aliasing of high-frequency noise into the region of interest (1 Hz to 10 kHz) and then sampled by a high-resolution ADC. Additional details of the EFD measurements are provided in Supplementary Section II and schematically in Supplementary Fig. 1. The time-domain samples were processed offline for spectral measurements and yielded the frequency noise and ADEV plots reported in Fig. 3d,e. Additional details of the ADEV measurements are provided in Supplementary Section III and Supplementary Fig. 2.

FLWs and ILWs. We used the measured frequency noise, $S_\nu(f)$, to calculate the FLW of each independent optical source. The FLW, also often referred to as the instantaneous or quantum-limited linewidth, gives rise to a laser's Lorentzian lineshape for a white-noise-only laser and can therefore be determined by extracting the white noise floor in the FN spectra at high frequencies, where environmental noise is no longer dominant. The FLW (in hertz) is then given as

$$\delta_\nu = \pi h_0 \quad (2)$$

where h_0 is the white noise floor of $S_\nu(f)$ in units of $Hz^2\,Hz^{-1}$.

The ILWs of the optical sources were calculated using two approaches, the β-separation method[40] and an integration of phase noise method[2,30]. The β-separation method is a modulation index approach to ILW calculation, accounting for the frequency noise components that contribute to lineshape broadening versus modulation that occurs at higher offset frequencies that does not increase ILW[40]. The second method[2,30] integrates phase noise from a carrier frequency offset of infinity (highest measured frequency offset, and such that the maximum frequency is much greater than the ILW) to the frequency offset at which the integral equals $1/\pi\,rad^2$. For a white-noise-only laser, this integration yields the offset frequency corresponding to the full-width at half-maximum (FWHM) of the laser lineshape. Additional details of ILW calculations are provided in Supplementary Section IV and schematically in Supplementary Fig. 3. Linewidth results are summarized in Supplementary Table 1.

Optical phase lock of CS-SBS lasers. One CS-SBS laser was transmitted over fibre and optically mixed with a tunable CS-SBS Rx laser. We achieved tunability of the Rx CS-SBS laser using an electro-optic modulator driven by a VCO to generate phase-modulated optical sidebands. Using a fibre Bragg grating optical filter, the upper sideband (USB) was filtered out and the carrier and lower sideband suppressed. By tuning the frequency of the VCO, the filtered CS-SBS USB is made tunable. The tunable CS-SBS USB is homodyne photomixed with the transmitted CS-SBS carrier signal on a balanced photodetector to generate a phase error signal[24] between the Tx and Rx lasers. The phase error signal passes through a PI^2D filter with integrator poles at 50 kHz and 100 kHz and fed back to the VCO control port to close the phase-locked loop. The lock-acquisition range[42,54] is estimated by detuning the initial frequency offset between the two lasers and attempting to engage closed-loop phase-locked operation with zero cycle slips. It was measured to be ~700 kHz, near the estimated servo loop bandwidth.

Residual phase error of the closed-loop OFS-PLL. For the phase lock performance results versus time and optical power in Fig. 4e, we measured the phase error signal during closed-loop operation, and we report the residual phase error variance[25], $\sigma_\phi^2\,rad^2$. We measured the peak-to-peak voltage, V_{pp}, of the open-loop homodyne signal (beat note between the two CS-SBS lasers near zero frequency detuning). During closed-loop operation, the phase error signal from the 45-MHz-bandwidth balanced photodiode r.m.s. voltage was measured on a digital storage oscilloscope for a time span of 2 s, sampled at 31.25 kHz, and V_{RMS} divided by V_{pp} and scaled by π (a half-cycle of the IF signal corresponds to V_{pp} and π-rad phase error) is the phase error r.m.s. in radians, or the phase error standard deviation for a signal with zero mean. The square of this is the reported residual phase error variance, σ_ϕ^2, in rad^2. The phase lock performance was measured in this manner for each of the data points in Fig. 4e over a timescale of 20 min for each received optical power.

Data availability

The data that support the plots within this paper and other findings of this study are available from the corresponding author on reasonable request.

References

54. Gardner, F. M. *Phaselock Techniques* 3rd edn (Wiley, 2005).

Acknowledgements

This research was supported by the OPEN 2018 Advanced Research Projects Agency–Energy (ARPA-E), US Department of Energy, under award no. DE-AR0001042. The views and conclusions contained in this document are those of the authors and should not be interpreted as representing official policies of ARPA-E or the US Government.

Author contributions

G.M.B., D.J.B. and S.B.P. prepared the manuscript. D.J.B. conceived the OFS-PLL approach. D.J.B., G.M.B., M.W.H. and S.B.P. conceived the implemented OFS-PLL architecture. P.A.M. contributed the narrow-linewidth integrated optical pump sources. D.B. fabricated the SiN integrated high-Q resonator SBS laser chip. W.Z., L.S. and S.B.P. contributed the optical cavity used in the SBS laser stabilization stage. G.M.B. and M.W.H. performed the experiments, including SBS generation, SBS stabilization to cavities and optical phase locking along with the associated noise and performance characterizations. J.H.D. and R.O.B. contributed simulations of laser noise, fibre noise and performance and identification of noise contributions from SBS and cavity stabilization physics theory. All authors contributed to analysing the simulated and experimental results. D.J.B. and S.B.P. supervised and led the scientific collaboration.

Competing interests

The authors declare no competing interests.

Additional information

Supplementary information The online version contains supplementary material available at https://doi.org/10.1038/s41566-021-00831-w.

Correspondence and requests for materials should be addressed to D.J.B.

Peer review information *Nature Photonics* thanks the anonymous reviewers for their contribution to the peer review of this work.

Reprints and permissions information is available at www.nature.com/reprints.